Multiple Exciton Collection in a Sensitized Photovoltaic System

Justin B. Sambur, *et al.*

Science **330**, 63 (2010);
DOI: 10.1126/science.1191462

nally, dynamical decoupling can be applied to protect entangled states, which are at the heart of quantum information science.

References and Notes

1. J. Clarke, F. K. Wilhelm, *Nature* **453**, 1031 (2008).
2. R. Hanson, D. D. Awschalom, *Nature* **453**, 1043 (2008).
3. D. Loss, D. P. DiVincenzo, *Phys. Rev. A* **57**, 120 (1998).
4. B. E. Kane, *Nature* **393**, 133 (1998).
5. L. Childress, J. M. Taylor, A. S. Sørensen, M. D. Lukin, *Phys. Rev. Lett.* **96**, 070504 (2006).
6. J. A. Jones *et al.*, *Science* **324**, 1166 (2009).
7. C. Degen, *Appl. Phys. Lett.* **92**, 243111 (2008).
8. J. M. Taylor *et al.*, *Nat. Phys.* **4**, 810 (2008).
9. W. H. Zurek, *Nat. Phys.* **5**, 181 (2009).
10. L. Viola, L. Knill, S. Lloyd, *Phys. Rev. Lett.* **82**, 2417 (1999).
11. D. Vitali, P. Tombesi, *Phys. Rev. A* **59**, 4178 (1999).
12. K. Khodjasteh, D. A. Lidar, *Phys. Rev. Lett.* **95**, 180501 (2005).
13. G. D. Fuchs, V. V. Dobrovitski, D. M. Toyli, F. J. Heremans, D. D. Awschalom, *Science* **326**, 1520 (2009).
14. Materials and methods are available as supporting material on *Science* Online.
15. L. Childress *et al.*, *Science* **314**, 281 (2006).
16. R. Hanson, V. V. Dobrovitski, A. E. Feiguin, O. Gywat, *Science* **320**, 352 (2008).
17. L. Jiang *et al.*, *Science* **326**, 267 (2009).
18. P. Neumann *et al.*, *Nat. Phys.* **6**, 249 (2010).
19. R. Hanson, L. P. Kouwenhoven, J. R. Petta, S. Tarucha, L. M. K. Vandersypen, *Rev. Mod. Phys.* **79**, 1217 (2007).
20. H. Bluhm *et al.*, http://arxiv.org/abs/1005.2995v1 (2010).
21. J. J. L. Morton *et al.*, *Nature* **455**, 1085 (2008).
22. J. Klauder, P. Anderson, *Phys. Rev.* **125**, 912 (1962).
23. G. S. Uhrig, *Phys. Rev. Lett.* **98**, 100504 (2007).
24. M. J. Biercuk *et al.*, *Nature* **458**, 996 (2009).
25. J. Du *et al.*, *Nature* **461**, 1265 (2009).
26. S. Pasini, G. S. Uhrig, *Phys. Rev. A* **81**, 012309 (2010).
27. L. Cywiński, R. M. Lutchyn, C. P. Nave, S. Das Sarma, *Phys. Rev. B* **77**, 174509 (2008).
28. T. Gullion, D. Baker, M. S. Conradi, *J. Magn. Reson.* **89**, 479 (1990).
29. M. A. Nielsen, I. L. Chuang, *Quantum Computation and Quantum Information* (Cambridge Univ. Press, Cambridge, 2000).

30. We acknowledge support from the Defense Advanced Research Projects Agency, the Dutch Organization for Fundamental Research on Matter (FOM), and the Netherlands Organization for Scientific Research (NWO). Work at the Ames Laboratory was supported by the U.S. Department of Energy Basic Energy Sciences under contract DE-AC02-07CH11358.

Supporting Online Material

www.sciencemag.org/cgi/content/full/science.1192739/DC1
Materials and Methods
Figs. S1 to S5
References

24 May 2010; accepted 19 August 2010
Published online 9 September 2010;
10.1126/science.1192739
Include this information when citing this paper.

Multiple Exciton Collection in a Sensitized Photovoltaic System

Justin B. Sambur,[1,2] Thomas Novet,[3] B. A. Parkinson[1]*

Multiple exciton generation, the creation of two electron-hole pairs from one high-energy photon, is well established in bulk semiconductors, but assessments of the efficiency of this effect remain controversial in quantum-confined systems like semiconductor nanocrystals. We used a photoelectrochemical system composed of PbS nanocrystals chemically bound to TiO_2 single crystals to demonstrate the collection of photocurrents with quantum yields greater than one electron per photon. The strong electronic coupling and favorable energy level alignment between PbS nanocrystals and bulk TiO_2 facilitate extraction of multiple excitons more quickly than they recombine, as well as collection of hot electrons from higher quantum dot excited states. Our results have implications for increasing the efficiency of photovoltaic devices by avoiding losses resulting from the thermalization of photogenerated carriers.

The urgent need for massively scalable carbon-free energy sources has focused attention on both increasing the efficiency and decreasing the cost of photovoltaic cells. When electrons are excited by photons with energy (E_{hv}, where h is Planck's constant and v is photon frequency) in excess of a semiconductor band gap, they tend to rapidly thermally relax to the conduction band edge; in this context, Shockley and Queisser calculated the maximum solar to electrical energy conversion efficiency for an optimal single band gap (E_g) semiconductor absorber to be about 31% (*1*). Third-generation solar cells have their basis in concepts that can potentially circumvent the so-called Shockley-Queisser limit (*2*). One such mechanism currently under active investigation (*3*–*5*) is to convert the excess energy of incident photons with $E_{hv} \geq 2E_g$ into additional free carriers in the material. An ideal material would produce two carriers per photon beginning at $E_{hv} = 2E_g$ and additional carriers for photons with energies equal to multiples of E_g [i.e., for $E_{hv} = 4E_g$, four carriers are generated per photon; however, 94% of the maximum gain in power conversion efficiency would be produced with just two carriers per photon (*6*)]. This process is known as carrier multiplication via impact ionization in bulk semiconductors but is quite inefficient because it usually requires E_{hv} to be much greater than $2E_g$ to generate an additional carrier per incident photon. However, there have been suggestions (*7*, *8*) that the process could be more efficient in semiconductor nanocrystals or quantum dots (QDs) because of the electronic structure associated with carrier confinement in three dimensions. In QDs, the process is known as multiple exciton generation (MEG) because the carriers are not free but instead are correlated as a result of confinement. Optical measurements of various nanomaterial systems, including colloidal QD solutions (*9*–*17*), QD thin films (*18*), and single-walled carbon nanotubes (SWCNT) (*19*), have identified signatures of MEG, but the generation efficiency in nanomaterials relative to bulk materials is still under discussion (*20*–*22*).

Despite numerous reports of optical detection of MEG in QDs, multiple exciton collection (MEC) from QDs, converting absorbed photons into photocurrents with quantum yields greater than one, has not yet been observed in a photovoltaic device. Recent reports measured MEG photocurrent in individual SWCNT photodiodes operating at low temperatures (*23*), separation of

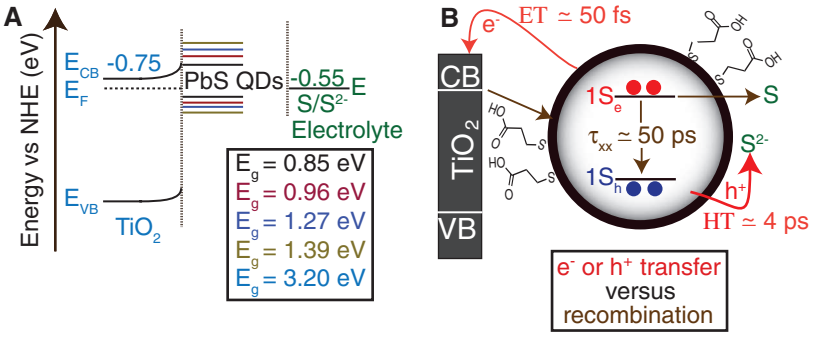

Fig. 1. Band energy diagram indicating the relevant energy levels and kinetic processes that describe PbS QD ET and HT into the TiO_2 conduction band and the sulfide/polysulfide electrolyte, respectively. (**A**) Energy-level alignment of the TiO_2 conduction band (*35*) with variously sized PbS QDs and the S/S^{2-} redox couple at pH 13. (Inset) The band gap energies of TiO_2 and the QDs used in this study. (**B**) Representation of a QD adsorbed on a TiO_2 single crystal and the approximate time scales for efficient ET and HT compared with the biexciton lifetime (τ_{xx}), as well as other possible recombination pathways. $1S_e$ and $1S_h$ refer to the first excited electron and hole state, respectively. Red and brown arrows indicate the favorable processes and the possible recombination pathways, respectively.

[1]Department of Chemistry and School of Energy Resources, University of Wyoming, Laramie, WY 80271, USA. [2]Department of Chemistry, Colorado State University, Fort Collins, CO 80523, USA. [3]Voxtel Incorporated, Beaverton, OR 97006, USA.

*To whom correspondence should be addressed. E-mail: bparkin1@uwyo.edu

multiexcitons generated by multiphoton absorption in colloidal CdSe QDs with physisorbed electron acceptors (*24*), and a photodetector made with PbS QDs that showed enhanced photoconductivity at higher photon energies attributed to MEG (*25*). High short-circuit photocurrents have been achieved in photovoltaic devices consisting of several-hundred-nm-thick layers of PbSe (*26*) or PbS (*27*, *28*) QDs, but quantum yields greater than unity have not been confirmed.

The dye-sensitized solar cell, a subject of intense research since its invention in 1991 (*29*), is a photoelectrochemical photovoltaic device that has the potential to be cost-effectively mass-produced. The most common manifestation of this device consists of a thin film of inexpensive nanocrystalline titanium dioxide that acts as both a charge-transporting substrate and a high-surface-area scaffold for attaching visible light-absorbing dye molecules (sensitizers) that inject photoexcited electrons into the TiO_2 conduction band. Recently QDs have been investigated as sensitizers because of their potential for enhanced stability compared with conventional dyes, as well as high light absorption cross sections that can be tuned to cover a large fraction of the solar spectrum simply by varying the particle size (*30*, *31*). Despite such beneficial attributes, quantum dot–sensitized solar cells (QDSSCs) have not achieved efficiencies or stabilities competitive with conventional dye-sensitized solar cells. One reason for this is that the surface chemistry for the chemical attachment of the QDs to the TiO_2 surface was not well understood or controlled. In several of our recent studies, we used single crystals of both anatase and rutile forms of TiO_2 as simple model systems to evaluate the influence of different QD attachment procedures on the electronic coupling of CdSe QDs and CdSe/ZnS core/shell QDs to the TiO_2 surface by measuring the photocurrent yields due to electron transfer from photoexcited QDs into TiO_2 (*32*, *33*). We used a surface chemistry strategy whereby short-chain, bifunctional passivating ligands such as 3-mercaptopropionic acid (MPA) stabilize the QDs in water while chemically binding the nanocrystals to the TiO_2 surface via thiolate and carboxylic acid moieties, respectively (*34*). Atomic force microscopy (AFM) confirmed that our surface chemistry strategy reproducibly resulted in a single layer of QDs covalently bound to the atomically flat single-crystal substrates with no three-dimensional QD clusters.

The minimum photon energy for observing MEG in CdSe or CdSe/ZnS QDs would be twice the bulk band gap (>3.4 eV). Considering that quantum confinement increases the band gap compared with the bulk, we decided to shift our focus to PbS, with a considerably lower bulk band gap value of 0.37 to 0.41 eV at 300 K (*35*). PbS QDs are readily synthesized with band gap energies ranging from 0.5 to 2.0 eV, making it possible to measure sensitized photocurrents associated with MEG by using photons sufficiently low in energy to preclude direct excitation of the TiO_2 band gap (3.0 eV for rutile and 3.2 eV for anatase).

The kinetically controlled pathways for photogenerated electrons and holes in a QDSSC are depicted in Fig. 1. Efficient production of sensitized photocurrents requires the energy of the QD excited state to be higher (more negative on the electrochemical scale) than the conduction band energy of the semiconductor substrate and well electronically coupled to the conduction band states of the semiconductor (Fig. 1A). After electron transfer (ET), the photooxidized QD is reduced by hole transfer (HT) to a redox species in solution with a reduction potential more negative than the ground state of the QD. In addition to the energetic constraints for efficient ET or HT, various recombination processes such as ET from the TiO_2 conduction band to the QDs (or electrolyte), as well as relaxation of the photoexcited electron to the QD ground state, compete with the forward processes (Fig. 1B). Therefore the ratio of rates of the forward (ET or HT) to the reverse (recombination) processes must be high enough to ensure that photocurrent generation is kinetically favored. Aside from the general recombination mechanisms inherent in QDSSCs, MEC requires very fast electron injection in order to outpace exciton-exciton annihilation. The measured fast electron injection times of <1 ns (*36*) and 50 fs (*37*) from photoexcited PbS and PbSe QDs, respectively, into TiO_2, as well as a 4-ps hole transfer time from PbS QDs to a solid-state organic hole acceptor (*38*), suggest that MEC can occur on a faster time scale than the 50-ps biexciton lifetime (τ_{xx}) measured in isolated PbS QDs (*39*) (Fig. 1B).

The structurally well-characterized interface of our electrolyte/PbS QD/single crystal TiO_2 system and the presence of a space charge field at the TiO_2 surface, which can quickly accelerate the injected electrons away from the interface, make this system particularly suitable to observe photocurrent collection from MEG in the adsorbed QDs. We synthesized (*34*) four QD samples with particle diameters of 9.9 ± 0.8 nm (standard deviation of transmission electron microscope data), 4.5 ± 0.3 nm, 3.1 ± 0.3 nm, and 2.5 ± 0.3 nm (fig. S1) with associated band gap energies (determined by the energy position in the absorbance spectra of the first exciton peak maxima) of 0.85 eV, 0.96 eV, 1.27 eV, and 1.39 eV, respectively. The semiconductor electrode is a nearly atomically flat anatase (001) surface that was imaged with AFM before and after exposure to MPA-capped PbS QDs. Figure 2A shows >100-nm terraces on the electrode surface before being uniformly coated by treatment with 4.5-nm MPA-capped PbS QDs [Fig. 2B; see also fig. S2 for QDs on rutile (001)]. The loose packing of the MPA-capped PbS QDs chemically linked to the TiO_2 surface suggests relatively smaller QD-QD interaction (or electronic coupling) when compared with a close-packed monolayer or multilayer films (*26*, *37*).

Because the alignment of the QD excited states relative to the TiO_2 conduction band is size-dependent (Fig. 1A), we used photocurrent spectroscopy to resolve the sensitized photocurrents as a function of incident photon energy for each QD size. We measured the light power at each incident photon energy to calculate the incident photon–to–current efficiency (IPCE) spectra (Fig. 3) from the sensitized photocurrents according to Eq. 1 (where c is the speed of light and λ is wavelength).

$$\mathrm{IPCE} = \frac{hc}{\lambda}\left[\frac{\text{photocurrent density } (\mu A/cm^2)}{\text{light power } (\mu W/cm^2)}\right] \quad (1)$$

The photocurrent response for QDs with E_g of 0.96 eV and larger (smaller diameter than 4.5 nm) showed distinct excitonic features at nearly the same photon energies observed in the absorbance spectra of the QDs suspended in water. Larger PbS QDs (E_g = 0.85 eV) did not sensitize the same anatase electrode at the energy of the first exciton because this excited state energy is more positive on the electrochemical scale than the TiO_2 conduction band energy (*28*, *40*, *41*). However, we observe sensitization from these QDs at 700 nm or 1.77 eV (Fig. 3A), indicating hot electron injection from higher QD excited states. A very recent study of PbSe QDs adsorbed on a rutile crystal in vacuum measured the time for hot electron injection to be extremely fast (50 fs) (*37*). Previous studies with similarly sized PbS QDs prepared by chemical bath deposition directly on

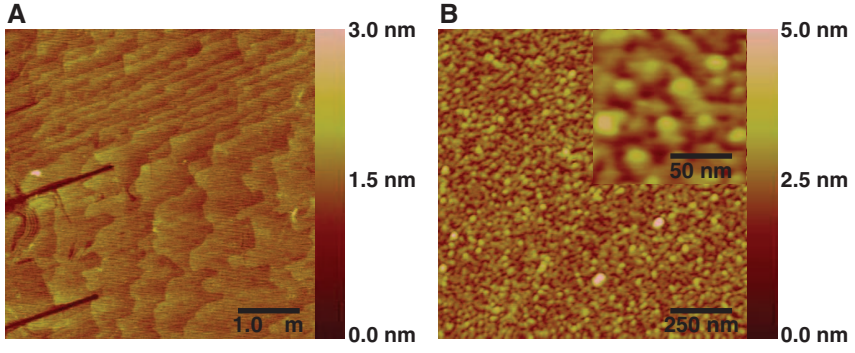

Fig. 2. AFM images of the anatase (001) electrode before and after the PbS QD adsorption procedure. (**A**) Bare electrode surface with an average terrace width of 350 nm with sporadic polishing damage indicated by ~2- to 5-nm grooves into the surface. (**B**) About-4.5-nm-diameter MPA-capped PbS QDs adsorbed on the same surface. (Inset) The loosely packed QDs at high resolution.

mesoporous TiO_2 films showed a photocurrent onset at about 800 nm or 1.5 eV (*42*), despite an onset of light absorption at ~1.2 eV. Thus, electron injection from the lowest excitonic states of PbS QDs into nanocrystalline TiO_2 was not observed previously in photocurrent spectra. This comparison suggests strong electronic coupling of PbS QD excited states to the TiO_2 conduction band in our system, resulting in facile charge injection and separation of the photoinjected electrons because of the space charge field present at the semiconductor-electrolyte interface. Therefore, multiple excitons produced from higher energy photons in the lowest energy PbS QD excited state should be collected as photocurrents with quantum yields greater than one.

For our planar electrodes covered with a single layer of QD sensitizers, the IPCE values are several orders of magnitude lower than those observed in typical sensitized mesoporous TiO_2 solar cells because of the low light absorption from the single layer of QDs. For this reason, the small photocurrent response in the near-infrared (IR) spectral region was acquired by using lock-in detection and a chopped monochromatic light source. Although this technique is very sensitive for measuring small photocurrent signals, the quantification of MEG effects requires accurate measurement of the absorbed photon–to–current efficiency (APCE, Eq. 2). APCE values take into account the light-harvesting efficiency (LHE; Eq. 3), or light actually absorbed by the monolayer of QDs.

$$\text{APCE (\%)} = \text{IPCE (\%)}/\text{LHE (\%)} \quad (2)$$

$$\text{LHE (\%)} = 1 - 10^{-\text{Absorbance}} \quad (3)$$

Accurate determination of APCE values required accurate measurements of both the optical absorbance of the QDs adsorbed on the TiO_2 surface and the steady-state short circuit photocurrents at various incident photon energies (fig. S3, A to C). The absorbance measurements were performed on undoped semitransparent rutile (001) TiO_2 single crystals with both sides polished (doped anatase and rutile crystals required for photocurrent measurements are not transparent) by using a dual-beam configuration in the ultraviolet-visible (UV-Vis) spectrometer (fig. S3D). Multiple regions of the rutile and anatase crystal surfaces, which were exposed to the same QD solutions at the same time, were imaged with AFM in order to assure that the densities of QDs on all the surfaces were nearly identical to those shown in Fig. 2B (also fig. S2). The absorbance spectra of the PbS QDs adsorbed on the rutile single crystal were similar to the solution absorbance spectra (fig. S4). Because of the larger band gap for the anatase polymorph compared with that of rutile (3.2 eV versus 3.0 eV), anatase was used for the MEC measurements to eliminate any contribution from direct excitation of TiO_2 to the sensitized photocurrent signal at the wavelengths where MEG would be expected.

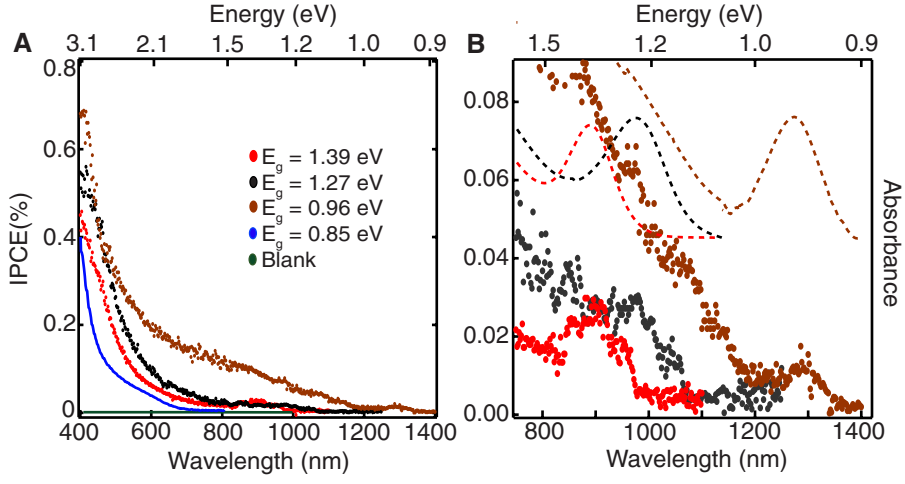

Fig. 3. IPCE spectra of various band gap PbS QDs adsorbed on an anatase (001) electrode. Photocurrents were acquired in an aqueous electrolyte (0.5 M Na_2S and 0.01 M S in 0.1 M NaOH) at short circuit in a two-electrode configuration versus a platinum wire. (**A**) IPCE spectra for each QD size. The green trace represents the bare anatase (001) photocurrent response. (**B**) IPCE spectra displaying the near-IR region to compare the photocurrent (solid dots) and QD absorbance in water (dashed lines).

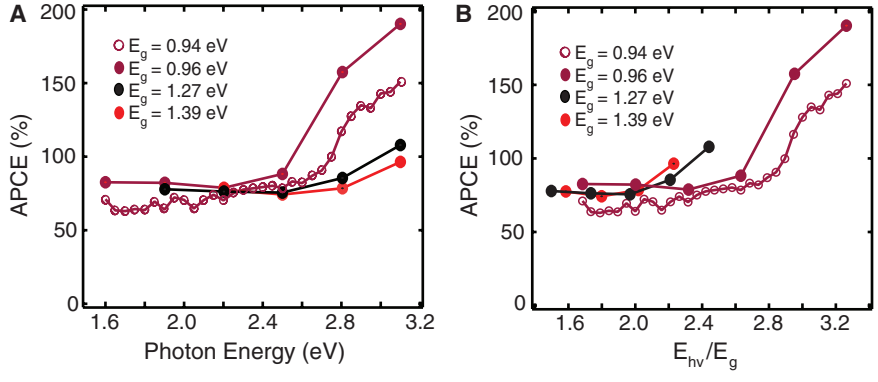

Fig. 4. APCE values as a function of the illumination energy. (**A**) APCE versus the absolute incident photon energy. (**B**) APCE versus the incident photon energy divided by the QD band gap energy (indicating the multiples of the band gap). Adjustments that would increase the APCE because of solution absorption and reflection from the cell window and TiO_2 crystal were not performed.

Figure 4, A and B, shows the calculated APCE values both as a function of excitation energy and the ratio of the excitation energy to the nanocrystal band gap (E_{hv}/E_g) for the three sizes of PbS QDs. The APCE values, not adjusted for solution absorbance or reflections from the cell window and crystal surface, remained nearly constant for each QD sample at 70 ± 13% [standard deviation of photocurrent data (*34*)] from 1.6 eV up to an absolute photon energy of 2.5 eV (Fig. 4A). No increase in the quantum yields indicative of MEC was observed despite crossing the threshold of illumination with photon energies of twice the band gap for the 4.5-nm PbS QDs (0.96 × 2 = 1.92 eV). However, at 2.8 and 3.1 eV illumination, the QDs with E_g = 0.96 eV (corresponding to photon energies of 2.9 and 3.2 times the band gap) exhibited APCE values that exceeded unity. There are also indications that APCE values, uncorrected for reflection and absorption losses, approach or exceed 100% at the highest photon energies for QDs with E_g = 1.27 and 1.39 eV; however, these values remain within the experimental error of the lower energy photocurrent measurements.

An additional sample of PbS nanocrystals with E_g = 0.94 eV was synthesized in order to ascertain any sample dependence (*43*) on the APCE yields (plotted in Fig. 4, A and B) and to more precisely map out the photon energy dependence of the MEC yields. The absolute magnitudes of the APCEs in this sample are smaller by 5 to 10% and 20 to 40% at photon energies in the non-MEC and MEC collection regions, respectively, but still nearly double at the higher (relative to lower) photon energies. We emphasize that in order to observe APCE values of over 100% the anatase electrode surface must not be contaminated and should exhibit large (>50 nm), nearly atomically flat terraces in AFM images. Therefore, in addition to any possible QD sample to sample variation in the MEC yields, we consider the condition of the electrode surface to be paramount in obtaining high and reproducible sensitized photocurrents.

There are conflicting reports regarding the energy threshold for MEG and the extent to which quantum yields exceed unity in quantum-confined systems in solution measured with optical methods (*43*). However, there are substantial differences between optically and photoelectrochemically measured MEG. MEC in our photoelectrochemical photovoltaic system is calculated from very straightforward measurements of steady-state currents, photon fluxes, and optical absorption. Detection of MEG in isolated colloidal QDs using ultrafast optical techniques requires complex data analysis and may be complicated by artifacts associated with trap states, charging of the QDs, and multiple-photon absorption in a single QD that could result in higher apparent MEG yields (*43*). The photocurrents we measured exhibited no short time scale transients associated with charge trapping and detrapping of carriers (fig. S3, A to C). Furthermore, steady-state MEC photocurrents (APCE = 170%) were sustained for 8 hours of continuous illumination with 4.3 $\mu W/cm^2$ of 3.1-eV incident photons; under these conditions, each QD undergoes nearly 1000 turnovers or on average about one multiple electron injection and collection every minute.

Although our >100% APCE values are higher and commence at slightly lower energy than the optically determined MEG yields for isolated colloidal PbS QDs (*10*), it was recently shown that the internal gain in PbS QD photoconductive photodetectors increased at E_{hv}/E_g = 2.7 and nearly doubled at E_{hv}/E_g = 3.2 (*25*). Despite the different mechanisms governing current flow in the two systems, the manifestation of MEG at similar values of E_{hv}/E_g and the similar magnitudes of the yields are notable. The lower bound of the APCE values for our PbS QDs, demonstrating MEC at an absolute incident photon energy of 3.1 eV, is about 15 to 30% greater than MEG yields for oleic acid–capped PbS QDs (E_g = 0.85 eV) in tetrachloroethylene that was studied optically by Nozik and co-workers (*10*). The different dielectric environment of MPA-capped PbS QDs adsorbed on TiO_2 is one possible cause for the difference in absolute magnitude between our APCE values and MEG yields reported in typical solution spectroscopic measurements (i.e., water and a TiO_2 surface versus QDs capped with long-chain hydrocarbon surfactants in nonaqueous solutions). However, it appears that onset of MEC occurs at about 2.5 ± 0.25 E_g for the QD sizes studied herein, in agreement with the onset of MEG determined optically with InP QDs with various band gaps (*14*). At present, optical measurements of MEG from PbS QDs capped with short-chain thiols in an aqueous medium are not available for direct comparison to our results.

The results presented herein are encouraging for the future design and development of photovoltaic devices that exploit MEG and MEC to surpass the Shockley-Queisser efficiency limit and approach the ideal single MEG absorber efficiency of 45% (*7*). However, it remains unclear to what extent MEC can improve the power conversion efficiency in a thin film or QD-sensitized device, especially if the onset of MEC is at nearly three times the QD band gap.

References and Notes

1. W. Shockley, H. J. Queisser, *J. Appl. Phys.* **32**, 510 (1961).
2. M. A. Green, *Third Generation Photovoltaics* (Bridge Printery, Sydney, Australia, 2001).
3. A. Shabaev, A. L. Efros, A. J. Nozik, *Nano Lett.* **6**, 2856 (2006).
4. V. I. Rupasov, V. I. Klimov, *Phys. Rev. B* **76**, 125321 (2007).
5. A. Franceschetti, J. M. An, A. Zunger, *Nano Lett.* **6**, 2191 (2006).
6. M. C. Hanna, A. J. Nozik, *J. Appl. Phys.* **100**, 074510 (2006).
7. A. J. Nozik, *Chem. Phys. Lett.* **457**, 3 (2008).
8. H. Benisty, *Phys. Rev. B* **51**, 13281 (1995).
9. D. Gachet, A. Avidan, I. Pinkas, D. Oron, *Nano Lett.* **10**, 164 (2010).
10. R. J. Ellingson *et al.*, *Nano Lett.* **5**, 865 (2005).
11. J. E. Murphy *et al.*, *J. Am. Chem. Soc.* **128**, 3241 (2006).
12. J. J. H. Pijpers *et al.*, *J. Phys. Chem. C* **111**, 4783 (2008).
13. R. D. Schaller, J. M. Pietryga, V. I. Klimov, *Nano Lett.* **7**, 3469 (2007).
14. M. T. Trinh *et al.*, *Nano Lett.* **8**, 1713 (2008).
15. S. K. Stubbs *et al.*, *Phys. Rev. B* **81**, 081303 (2010).
16. M. Ji *et al.*, *Nano Lett.* **9**, 1217 (2009).
17. Y. Kobayashi, T. Udagawa, N. Tamai, *Chem. Lett.* **38**, 830 (2009).
18. M. C. Beard *et al.*, *Nano Lett.* **9**, 836 (2009).
19. S. Wang, M. Khafizov, X. Tu, M. Zheng, T. D. Krauss, *Nano Lett.* **10**, 2381 (2010).
20. G. Nair, S. Geyer, L. Chang, M. Bawendi, *Phys. Rev. B* **78**, 125325 (2008).
21. C. Delerue, G. Allan, J. J. H. Pijpers, M. Bonn, *Phys. Rev. B* **81**, 125306 (2010).
22. M. Ben-Lulu, D. Mocatta, M. Bonn, U. Banin, S. Ruhman, *Nano Lett.* **8**, 1207 (2008).
23. N. M. Gabor, Z. Zhong, K. Bosnick, J. Park, P. L. McEuen, *Science* **325**, 1367 (2009).
24. J. Huang, Z. Huang, Y. Yang, H. Zhu, T. Lian, *J. Am. Chem. Soc.* **132**, 4858 (2010).
25. V. Sukhovatkin, S. Hinds, L. Brzozowski, E. H. Sargent, *Science* **324**, 1542 (2009).
26. J. M. Luther *et al.*, *Nano Lett.* **8**, 3488 (2008).
27. J. Tang *et al.*, *ACS Nano* **4**, 869 (2010).
28. A. G. Pattantyus-Abraham *et al.*, *ACS Nano* **4**, 3374 (2010).
29. B. O'Regan, M. Grätzel, *Nature* **353**, 737 (1991).
30. G. Hodes, *J. Phys. Chem. C* **112**, 17778 (2008).
31. P. V. Kamat, *J. Phys. Chem. C* **112**, 18737 (2008).
32. J. B. Sambur, S. C. Riha, D. Choi, B. A. Parkinson, *Langmuir* **26**, 4839 (2010).
33. J. B. Sambur, B. A. Parkinson, *J. Am. Chem. Soc.* **132**, 2130 (2010).
34. Materials and methods are detailed in supporting material on *Science* Online.
35. W. H. Strehlow, E. L. Cook, *J. Phys. Chem. Ref. Data* **2**, 163 (1973).
36. H. C. Leventis *et al.*, *J. Am. Chem. Soc.* **132**, 2743 (2010).
37. W. A. Tisdale *et al.*, *Science* **328**, 1543 (2010).
38. R. Plass, S. Pelet, J. Krueger, M. Grätzel, U. Bach, *J. Phys. Chem. B* **106**, 7578 (2002).
39. E. Istrate *et al.*, *J. Phys. Chem. B* **112**, 2757 (2008).
40. B.-R. Hyun *et al.*, *ACS Nano* **2**, 2206 (2008).
41. D. Dissanayake, T. Lutz, R. J. Curry, S. R. P. Silva, *Appl. Phys. Lett.* **93**, 3 (2008).
42. H. Lee *et al.*, *Adv. Funct. Mater.* **19**, 2735 (2009).
43. J. A. McGuire, J. Joo, J. M. Pietryga, R. D. Schaller, V. I. Klimov, *Acc. Chem. Res.* **41**, 1810 (2008).

44. We thank M. G. Bawendi, A. J. Nozik, and D. P. Shepherd for helpful discussions. J.B.S. and B.A.P. acknowledge U.S. Department of Energy–Basic Energy Sciences grant no. DE-FG03-96ER14625 for funding. T.N. acknowledges Department of Energy grant no. DE-FG36-08GO18025 for financial support.

Supporting Online Material

www.sciencemag.org/cgi/content/full/330/6000/63/DC1
Materials and Methods
SOM Text
Figs. S1 to S4
Tables S1 to S4
References

26 April 2010; accepted 13 August 2010
10.1126/science.1191462

Allosteric Supramolecular Triple-Layer Catalysts

Hyo Jae Yoon, Junpei Kuwabara,* Jun-Hyun Kim,† Chad A. Mirkin‡

Allosteric regulation of organometallic catalysts could allow for greater control over reactions. We report an allosteric supramolecular structure in which a monometallic catalytic site has been buried in the middle layer of a triple-layer complex. Small molecules and elemental anions can open and close this complex and reversibly expose and conceal the catalytic center. The ring-opening polymerization of ε-caprolactone can be turned on by the in situ opening of the triple-layer complex and then completely turned off by reforming it through the abstraction of Cl^-, the allosteric effector agent, without appreciable loss of catalytic activity. This process can regulate the molecular weights of the resulting polymers.

Supramolecular coordination complexes, in which multiple weak bonding interactions control structure, have found several applications, including catalysis (*1*–*7*), recognition of small molecules (*8*–*11*), and facilitated small-molecule transport (*12*). Such systems can encapsulate molecules (*3*), and the nanoscale environment created by a supramolecular complex can increase the speed of a chemical reaction (*4*, *5*), alter reaction routes (*6*), control stereochemistry (*5*), affect oligomerization processes (*7*), or extend the lifetimes of highly reactive molecules such as cyclobutadiene (*13*). An important goal is to regulate the activity of catalysts through the addition of small molecules that change the supramolecular structure of the catalyst and in turn control catalytic reaction rates and product distributions (*14*–*17*), much like the behavior of many allosteric enzymes. Herein, we present a proof-of-concept example of such regulation for a living polymerization catalyst and demonstrate control over polymer growth and molecular weight.

There are three general methods for synthesizing supramolecular coordination complexes (*18*),